Decoupling of estuarine hypoxia and acidification as revealed by historical water quality data

Chunqi Shen[1,2*], Jeremy M. Testa[2], Maria Herrmann[3], Raymond G. Najjar[3]

[1]College of Environmental Science and Engineering, Suzhou University of Science and Technology, Suzhou, Jiangsu, 215224, China

[2]Chesapeake Biological Laboratory, University of Maryland Center for Environmental Science, Solomons, MD, 20688, USA

[3]Department of Meteorology and Atmospheric Science, The Pennsylvania State University, University Park, PA, 16802, USA

* *Corresponding author: Chunqi Shen* cshen@umces.edu

Abstract

Hypoxia and acidification are commonly coupled in eutrophic aquatic environments because aerobic respiration is usually dominant in bottom waters and can lower dissolved oxygen (DO) and pH simultaneously. However, the degree of coupling, which can be weakened by non-aerobic respiration and $CaCO_3$ cycling, has not been adequately assessed. In this study, we applied a mass-balance box model to 20 years of water quality monitoring data to explore the relationship between hypoxia and acidification along the mainstem of Chesapeake Bay. In the early summer, dissolved inorganic carbon (DIC) production in mid-bay bottom waters was dominated by aerobic respiration, contributing to DO and pH declines. In contrast, late-summer DIC production was higher than that expected from aerobic respiration, suggesting potential buffering processes, such as calcium carbonate dissolution, which would elevate pH in hypoxic/anoxic waters. These findings are consistent with contrasting seasonal relationships between riverine nitrogen (N) loads and hypoxic and acidified volumes. The N loads were associated with increased hypoxic and acidified volumes in June, but only increased hypoxic volumes in August, when acidified volume declines instead. Our study reveals that the magnitude of this decoupling varies interannually with watershed nutrient inputs, which has implications for the management of co-stressors in estuarine systems.

Keywords: Hypoxia, acidification, box model, Chesapeake Bay, estuary, carbonate chemistry.

Synopsis Statement: Excess nutrient loading leads to high pH-buffering processes in late summer that decouple hypoxia and acidification in the mainstem of Chesapeake Bay.

Graphic for Table of Contents:

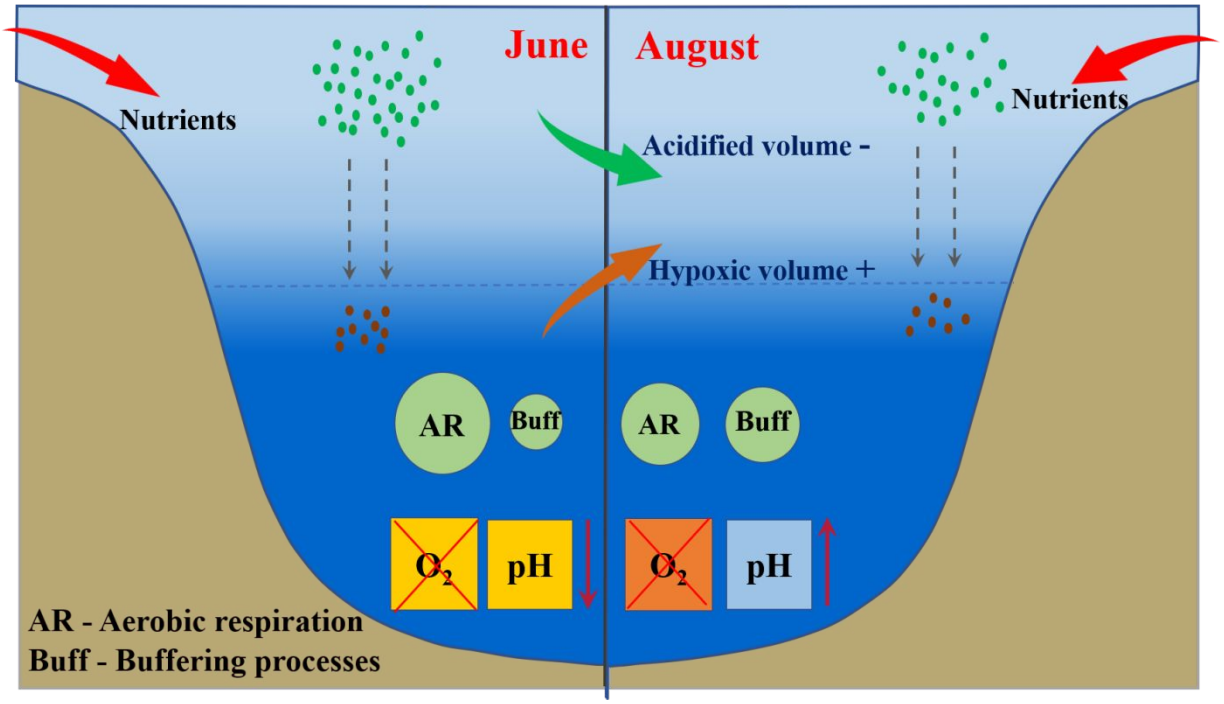

Introduction

Ocean acidification occurs at a global scale driven by the oceanic uptake of approximately one third of the anthropogenic carbon dioxide (CO_2) emissions and is rapidly changing the carbonate chemistry of the world oceans with increases in dissolved inorganic carbon (DIC) and decreases in pH and aragonite saturation state (Ω_{ar}).[1-3] Estuaries and coastal regions around the world are critical natural habitats for many ecologically and economically important species.[4] A large number of these regions are particularly vulnerable to acidification given inputs of poorly buffered freshwater[5-7] and/or stratification that can allow bottom-water DIC accumulation. Recent studies demonstrated that coastal acidification could be exacerbated by eutrophication through enhanced bottom respiration of allochthonous and autochthonous organic matter.[8,9] In fact, long-term field observational studies suggest that pH and Ω_{ar} decline faster in estuarine waters compared with the open ocean, where the decline is attributable mostly to the rising atmospheric CO_2.[10]

Hypoxia has been widely reported and studied across multiple estuaries and coastal regions around the world including the Baltic Sea,[11,12] the northern Gulf of Mexico,[13,14] the Pearl River,[15,16] and Chesapeake Bay.[17] Links between hypoxia and eutrophication have been well recognized through studies across diverse aquatic systems.[18-20] The two primary factors contributing to hypoxia are net biogeochemical dissolved oxygen (DO) consumption due to aerobic respiration and restricted supply of oxygen from the surface layer due to a lack of physical mixing.[21] Hypoxia and acidification are commonly coupled, i.e., display similar spatial and seasonal dynamics in eutrophic and stratified ecosystems, where aerobic respiration is the dominant process to lower both pH and DO of subsurface waters.[8,22,23] However, the duration, coverage and intensity of estuarine acidification, compared with hypoxia, is more challenging to predict because pH in estuarine waters responds to a series of physical and biogeochemical processes affecting carbonate chemistry variables, such as DIC and total alkalinity (TA), including anaerobic respiration (e.g., sulfate reduction), mixing with poorly buffered freshwater, and carbonate mineral precipitation and dissolution.[22,24,25]

Chesapeake Bay, the largest estuary in the contiguous United States, experiences both hypoxic and acidified conditions and has a wealth of long-term observations that provide the opportunity to explore oxygen and carbonate chemistry dynamics and drivers. Retrospective

analyses of 25-year (1984-2008) historical pH data in Chesapeake Bay suggested a potential long-term pH decline in polyhaline waters that was higher than expected from anthropogenic-CO_2-induced acidification alone.[10] Recent observational and modeling studies in the Bay have suggested potential explanations for non-anthropogenic CO_2 effects, resulting from strong spatiotemporal variability in carbonate chemistry driven by both external forcing (e.g., riverine DIC, TA, and nutrient changes) and internal cycling (e.g., $CaCO_3$ dissolution and H_2S oxidation), thus challenging our understanding of estuarine acidification and how it co-varies with hypoxia.[26-29] For example, Su et al.[30], using a single year of data in Chesapeake Bay bottom waters, suggested that supply-controlled $CaCO_3$ dissolution elevated pH while oxygen remained low. It remains unclear, however, how year-to-year changes in external forcing influence this decoupling at a bay-wide scale. Recent model simulations also indicated an important buffering mechanism of calcium carbonate dissolution for pH changes in late summer,[28] although the calcium precipitation/dissolution and the mineral sources in estuarine environments have not been clearly revealed. It remains challenging to accurately estimate the internal biogeochemical production rates, and to determine the underlying mechanisms of variable biogeochemical processes in regulating the seasonal and interannual variability of DO and pH. Thus, despite substantial progress towards understanding estuarine carbonate system dynamics, previous studies have relied on limited data to estimate rates of biogeochemical transformations causing changes in inorganic carbon cycling and oxygen cycling, and few have considered long-term variability in these rates and their implications for variability in acidification.

To address the above knowledge gap, the objective of this study is to assess seasonal and interannual variability in net biogeochemical transformations of DO and DIC in the mainstem Chesapeake Bay and explore the long-term relationship between hypoxia and acidification. We analyzed a 20-year (1999–2018) record of DO (directly measured) and DIC (computed from directly measured pH and modeled TA) along the mainstem of Chesapeake Bay using a box model, which has been successfully applied to investigate physical and biogeochemical dynamics in Chesapeake Bay.[31,32] Box model calculations are data driven and permit the computation of net biogeochemical rates that control the spatial and temporal dynamics of chemical species of interest (DO and DIC in the present study). We focused the model

application on processes regulating hypoxia and acidification, particularly in mid-bay bottom waters, where extremely low DO and pH were observed during summer. The mainstem acidified volumes were estimated for the first time by interpreting historical bay-wide water quality data, and the seasonal and interannual variability of the acidified and hypoxic volumes were examined to assess the relationships between the two metrics. We show that hypoxia and acidification in the mainstem of Chesapeake Bay are decoupled in late summer, when non-aerobic-respiration processes (all other biogeochemical processes but aerobic respiration, i.e., $CaCO_3$ dissolution, sulfate reduction) frequently occur and appear to buffer acidified bottom waters.

Materials and Methods

Study site

Chesapeake Bay, located in the United States mid-Atlantic coastal region, has a total length of 320 km from the mouth of the Susquehanna River to its outlet in the Atlantic Ocean (Fig. 1). The average depth is 6.5 m and a 20–35 m deep central channel runs the length of the middle region of the Bay. Water circulation in the mainstem is a typical two-layer pattern driven primarily by the surface movement of freshwater from the north and bottom intrusion of seawater from the south.[33] The Bay once supported abundant native oyster populations in the 19th century, but these have declined to just a few percent of the previous values due to overfishing, disease, habitat destruction, and water quality deterioration.[34] The Bay and its tributaries have been persistently eutrophic over the past 30 years, but some regions of the estuary have experienced modest improvements in overall water quality due to restrictions of nutrient inputs and ecosystem restoration efforts.[35,36]

Hypoxia has been documented throughout the past century in Chesapeake Bay and its tributaries.[37] The water below the pycnocline in the central mid Bay is particularly vulnerable to hypoxia during May–September when stratification is fully established and surface primary production is relatively high, leading to rapid bottom DO consumption by aerobic respiration in bottom waters[31,37] and sediments[38,39] without sufficient replenishment. The mid-bay hypoxic region is also typically acidified,[26] because of a combination of high DIC production

resulting from high rates of aerobic respiration in sediments and overlying waters,[28] and limited mixing with low-DIC surface waters caused by stratification.

Long-term water quality observations

Measurements of water column pH, temperature, salinity and DO were obtained from the water quality database of the Chesapeake Bay Program (CBP) (http://data.chesapeakebay.net). CBP data collection in the mainstem is organized into cruises or periods of time with coordinated sampling by the states of Maryland and Virginia. The field observations have generally been conducted once per month from November to February and twice per month from March to October since 1985, covering more than 50 mainstem stations with vertical profiles reported at a resolution of 1–2 m. We selected 21 regularly monitored stations along the central axis of the mainstem, seeking good spatial coverage while avoiding overrepresentation of stations clustered together, for use in a box model and in calculations of hypoxic volume and acidified volume (Fig. 1). Comparably high differences in long-term pH trends between stations measured by the state of Virginia and those measured by the state of Maryland have been found, and a detailed examination of data from adjacent monitoring stations (CB5.3 and CB5.4, Fig. 1) measured by the two states revealed a distinct separation before 1998 and convergence thereafter. Although the ultimate reason for these differences is uncertain, we limited our analysis to 1999–2018 to assure data accuracy and consistency.

Modeling of total alkalinity and dissolved inorganic carbon

DIC and TA are two key state variables for carbonate chemistry and are particularly useful for process modeling because they are conservative with respect to changes in temperature, salinity, and pressure (unlike pH and Ω_{ar}). However, while pH has been consistently measured at a bay-wide scale since 1985, DIC has been rarely measured in Chesapeake Bay until very recently and TA has been measured only at a limited number of stations and times. Therefore, we used a modeling approach to estimate TA and DIC from available long-term water quality observations.

Prior field measurements in the Bay and its tributaries have revealed a variety of patterns of TA along the salinity gradient,[26,27] and several studies have demonstrated a relatively linear

relationship between TA and salinity.[5,40,41] In this study, we adapted an empirical model of TA in the mainstem Bay from Herrmann et al.[42] Specifically, TA is modeled as a function of measured estuarine salinity and temporally varying riverine TA, assuming conservative mixing of two main sources of water for the mainstem Bay: Atlantic Ocean shelf (high-salinity source) and the Susquehanna River (USGS gage number 01578310, zero-salinity source). Because the model configuration reported in Herrmann et al.[42] was fit to surface salinity observations only, for this study we refit the model to include salinity observations from all available depths. The uncertainty in the mixing model was assessed using high-quality measurements of TA during 2016–2018 cruises.[27,40] The model captures the substantial effects of the seasonality and long-term increase in Susquehanna River TA on TA in the mainstem Bay. The refit empirical model was used to generate vertical profiles of TA at the 21 stations used in the present study.

A 200-member Monte Carlo ensemble of DIC was computed from observed CBP pH, temperature, salinity, and modeled TA corrected for organic alkalinity, by propagating the measurement uncertainty in pH (0.2 standard pH units, NBS), the uncertainty in modeled TA, and the uncertainty in the assumed organic alkalinity contribution (20 ± 30 μM) as described in Herrmann et al.[42] Ω_{ar} was also computed to contextualize some of the results. Computations were done at each station at the native time and depth resolution using CO2SYS.[43] We used the carbonic acid equilibrium constants of Cai and Wang,[44] the equilibrium constant for bisulfate ion of Dickson,[45] and the ratio of total boron to salinity of Uppström.[46] The phosphate and silicate concentrations were assumed to be zero; we also assumed that the zero-salinity end member has a zero calcium ion concentration, an assumption that leads to a minimal bias in calculated Ω_{ar} along the salinity gradient of the mainstem.

Box model description

The mainstem of Chesapeake Bay was divided into 9 regions, with the most landward region containing one box and the remaining eight segments each containing surface and bottom-layer boxes to represent the mean 2-layer circulation in the estuary (Figs. 1 and S1). The horizontal and vertical boundaries separating adjacent boxes were determined based on data availability, density stratification, and an effort to retain similar salinity gradients and

water volumes among boxes. Each box was assumed to be well mixed. Salinity, DO, and DIC at the 21 stations were first interpolated to a two-dimensional depth–length grid (~1 m x 2 km, Fig. S2) along the mainstem assuming the concentrations were uniform laterally. The interpolation method used is ordinary kriging,[47] in which the parameters of smoothness, sill and distance range were configured as 1.0, 9.0 and 120 km, respectively. Mean solute concentrations for each box and each month were computed as the volume-weighted means.

Circulation

Advective and non-advective water exchanges between neighboring boxes were calculated using the solution to non-steady state equations balancing salt and water mass given their independence from biogeochemical changes. The largest tributaries to the mainstem Bay (Figs. 1 and S1) were included implicitly as surface layer inputs of freshwater to Region 1 (Susquehanna), Region 2 (Patapsco), Region 5 (Patuxent), Region 6 (Potomac), Region 7 (Rappahannock), Region 8 (York), and Region 9 (James). Monthly average streamflow and salinity of tributaries were obtained from the nearby USGS gages and stations of CBP (Fig. 1 and Table S1).

The salt and water balances for each surface-layer box are, respectively:

$$V_{ti}\left(\frac{dS_{ti}}{dt}\right) + V_i\left(\frac{dS_i}{dt}\right) = Q_{i-1}S_{i-1} + Q_{vi}S'_i - Q_iS_i + E_{vi}(S'_i - S_i) \quad (1)$$

$$0 = Q_{i-1} + Q_{vi} - Q_i + Q_{fi} \quad (2)$$

where i represents the region number; V_i and V_{ti} are the volumes of the surface box and the adjacent tributary, respectively; S_i, S'_i and S_{ti} are the salinity in the surface box, bottom box and tributary, respectively; Q_i is the seaward horizontal advective transport; Q_{vi} is the vertical transport; Q_{fi} is the freshwater input; and E_{vi} is the vertical diffusion term. Similarly, the balance equations for bottom-layer boxes can be expressed as:

$$V'_i\left(\frac{dS'_i}{dt}\right) = Q'_{i+1}S'_{i+1} - Q_{vi}S'_i - Q'_iS'_i - E_{vi}(S'_i - S_i) \quad (3)$$

$$0 = Q'_{i+1} - Q_{vi} - Q'_i \quad (4)$$

where V'_i is the bottom box volume and Q'_i is the bottom landward transport. For this conservative model, salinity data were obtained from the CBP database as mentioned in the above section. Precipitation and evaporation are not included in the water balance assuming that direct precipitation to the water surface was approximately balanced by evaporation. All

time derivatives were computed using explicit centered difference method. The conservative tracer equations (Eqs. 1–4) are mathematically closed, and the advective and non-advective fluxes terms can be calculated.

Net biogeochemical production

We computed monthly rates of physical transport and net biogeochemical production of DO (P_{DO}) and DIC (P_{DIC}) for each box of the mainstem from 1999 to 2018. Physical transport rates for these non-conservative state variables were directly computed by multiplying the mean solute concentrations for each box and month by the advective and non-advective transports. The net biogeochemical production rates for surface and bottom boxes were derived based on mass balance equations:

$$P_i = V_i\left(\frac{dC_i}{dt}\right) - Q_{i-1}C_{i-1} - Q_{vi}C'_i + Q_iC_i - E_{vi}(C'_i - C_i) - Airsea \quad (7)$$

$$P'_i = V'_i\left(\frac{dC'_i}{dt}\right) - Q'_{i+1}C'_{i+1} + Q_{vi}C'_i + Q'_iC'_i + E_{vi}(C'_i - C_i) \quad (8)$$

where P_i and P'_i are the surface and bottom net production rates, C is the solute concentration, and $Airsea$ is the water-air exchange of O_2 or CO_2, which was calculated using:

$$F_{O2} = K_{O2} \times (O_{2,sat} - O_{2,water}) \quad (9)$$

$$F_{CO2} = K_{CO2} \times K \times (pCO_{2,air} - pCO_{2,water}) \quad (10)$$

where $O_{2,sat}$ is the saturation concentration of O_2,[48] K is the solubility of CO_2 from Weiss,[49] $pCO_{2,air}$ is the atmospheric CO_2 partial pressure measured at the Mauna Loa Observatory (https://gml.noaa.gov/ccgg/trends/mlo.html), and K_x is the gas transfer velocity for gas x (O_2 or CO_2) from Wanninkhof,[50]

$$K_x = 0.251 \times u_{10}^2\sqrt{\frac{660}{Sc_x}} \quad (11)$$

In Equation 11, K_x has units of cm hr^{-1}, u_{10} is the 10-m height wind speed in m s^{-1}, which is measured at the Patuxent River Naval Air Station (KNHK, 38.5N, 76.7W), and Sc_x is the temperature-dependent Schmidt number for a salinity of 35. We did not estimate the role of sediment–water exchange in the box-model calculations, as these rates are subsumed in the estimates of bottom-layer net production rates. Exchanges of DIC and DO between surface mainstem boxes and tributaries were ignored as field measurements of carbonate chemistry state variables in tributaries are particularly limited, and our analysis is primarily focused on

the bottom-water rates. The box model codes were generated, tested and run in the Matlab platform.

In this study, DIC production from aerobic respiration ($P_{DIC,\ aerobic}$) was calculated by multiplying the net biogeochemical consumption of DO (P_{DO}) with a stoichiometric O_2:C ratio of 106:138 ($P_{DIC,\ aerobic} = -0.768 \times P_{DO}$) assuming NO_3 as the main nitrogen source for phytoplankton.[51] DIC production from processes other than aerobic respiration was obtained by the difference ($P_{DIC,\ non\text{-}aerobic} = P_{DIC} - P_{DIC,\ aerobic}$). We restricted our biogeochemical production analysis to the summer period (May–September), when hypoxia occurs in Chesapeake Bay. We further divided the summer period into the early summer (May–June) and late summer (July–September), to explore temporal variations in the coupling and decoupling of hypoxia and acidification. Although we recognize that biogeochemical processes evolve continuously over time, sometimes including lags between linked productive and consumptive processes, dividing our data into discrete periods of time was a convenient way to track seasonal change.

Hypoxic and acidified volume

Several prior studies have examined the seasonal and annual hypoxic volumes in Chesapeake Bay and their relationship to freshwater flows and associated nutrient loads that regulate the intensity of stratification and bay-wide primary production and organic matter mineralization.[19,37] The seasonal and interannual variations of acidified volume in Chesapeake Bay, however, have yet to be discussed. We estimated the long-term hypoxic (DO < 62.5 μM) and acidified (pH < 7.5 NBS) volumes of the mainstem across the summer with spatially interpolated pH and DO data as mentioned in the above section. These volumes were related to freshwater flow and dissolved inorganic nitrogen loading from the Susquehanna River averaged over the months of January to May (winter and spring), considering that several previous analyses have related summer hypoxic volumes to be significantly dependent on winter–spring average discharge,[19,37] and the accumulation of phytoplankton biomass during spring was noted as the principal source of organic carbon that is decomposed in bottom waters during summer.[52]

Results and Discussion

Variations of observed monthly average concentrations of DO and DIC in the middle of Chesapeake Bay (Region 5) allow inferences about key drivers of seasonal variability of organic matter cycling (Fig. 2). Surface DO concentrations were maintained at relatively high levels, likely due to rapid exchange with the overlying atmosphere, and seasonal DO minima in summer follow reductions in oxygen saturation associated with high water temperature. Extremely low DO concentrations in bottom waters during summer were observed, reaching as low as 15.0 μM in July on average and the mid Bay consistently experienced hypoxia (DO < 62.5 μM) and anoxia (DO < 6.25 μM) during summer. Mean bottom-water DIC in the mid Bay peaked in the summer, presumably as a result of net biogeochemical production and weak vertical mixing between the surface and bottom layers. In this region, high rates of both sediment and water-column metabolism have been previously reported during summer,[31,53] a time when various estimates of stratification strength reach peak values.[19]

We focus the discussion of the box model results on the mean annual cycle, to place more emphasis on seasonal variability, and in mid-bay bottom waters, where hypoxia and acidification are most pronounced. Box-model net production rates indicated peaks in mid-bay bottom respiration (i.e., net DO consumption and DIC production) during April and May (Regions 4–6, Fig. 3a–c). The high respiration rate in spring is associated with high concentrations of DO (e.g., non-limiting) and particulate organic carbon (POC), the latter accumulating from the productive surface layer (with an average POC of 258 μM in May vs. 155 μM in July, Fig. S3). In contrast, net bottom-water DO consumption rates were very low in summer, particularly during August, when oxygen concentrations were near-zero and strong stable stratification greatly impeded the replenishment of bottom-water oxygen consumed in early summer. DO consumption rates increased with the breakdown of stratification in fall and the replenishment of DO associated with high rates of vertical mixing. The monthly biogeochemical production rates of DIC (P_{DIC}) generally followed the patterns of DO (P_{DO}) given that respiration is the dominant biogeochemical process in controlling the dynamics of DIC,[28] although other processes such as dissolution and sulfate reduction could also contribute to bottom DIC production under anoxic or low aragonite saturation conditions.

The uncertainty of P_{DIC} illustrated from the Monte Carlo ensemble was small, and the 20-year long-term monthly-average further diminished the variability (shaded area, Fig. 3a–c).

Our model results showed that the mean annual cycle of bottom $P_{DIC,\ non\text{-}aerobic}$ was nearly uniformly positive in bottom waters of the mid Bay (Fig. 3a–c). $P_{DIC,\ non\text{-}aerobic}$ was relatively high in July for Region 4 and 6, and in September for Region 5, months that are both within the typical hypoxic period between May to September. In comparing the long-term mean seasonal net production rates ($P_{DIC,\ non\text{-}aerobic}$ and $P_{DIC,\ aerobic}$), $P_{DIC,\ aerobic}$ accounted for approximately 65% of P_{DIC} in mid-bay bottom waters (slope of linear fit of P_{DIC} vs. $P_{DIC,\ aerobic}$, Fig. 3d), which is consistent with the ratio (~60%) estimated with a two end-member mixing model of Chesapeake Bay.[54] We further derived the ratios for early and late summer individually. The best fit lines suggested a higher ratio (71%) in early summer compared with that (60%) in late summer (Fig. 3d), implying a more dominant contribution of aerobic respiration to P_{DIC} in early summer when other DIC generation processes (e.g., sulfate reduction and mineral dissolution) are relatively weak. It has to be mentioned that the empirically-modeled TA we used in this analysis was relatively conservative to salinity, but recent observational studies have shown non-conservative behavior of TA associated with processes beyond aerobic respiration.[26,30] We used limited 1-year observed, non-conservative TA in the box model and found ~15% higher rates of $P_{DIC,\ non\text{-}aerobic}$, suggesting that our approach may be biased. Future work with a new set of TA observations could help constrain this source of uncertainty.

Carbonate mineral precipitation and dissolution can influence water column pH. Mechanisms of dissolution and precipitation have not been well explored and quantified in estuarine environments, despite recent implications of substantial effects in Chesapeake Bay.[5,25] We examined the relationship between aragonite saturation and $P_{DIC,\ non\text{-}aerobic}$ in the mid Bay (Fig. 4). The surface water displayed an overall net DIC consumption from non-aerobic processes associated with high aragonite saturation state, while net DIC production co-occurred with low saturation state in bottom waters. The vertical spatial patterns of $P_{DIC,\ non\text{-}aerobic}$ are consistent with the carbonate mineral processes, where precipitation is thermodynamically favored under higher saturation state and dissolution is favored under lower saturation state,[55] and $\Omega_{ar} = 1$ is commonly referenced as an abiotic

threshold for precipitation and dissolution (i.e., precipitation is thermodynamically favored when $\Omega_{ar} > 1$, while dissolution is favored when $\Omega_{ar} < 1$). Exponential functions were used to fit the non-aerobic-respiration DIC production with aragonite saturation state, and our results indicated an average threshold of 0.64 (0.59-0.70 for the Monte Carlo ensemble, Fig. 4) rather than 1.0 for the middle mainstem. A consideration of this alternative threshold value could help to identify habitat environments for shell-forming species in Chesapeake Bay, and to inform empirical and process-based models of mineral dissolution and precipitation in estuarine environments. Specifically, existing carbonate biogeochemistry models in Chesapeake Bay either do not fully consider calcium carbonate processes[29,56] or apply conventional saturation state thresholds initially derived and widely used in coastal and open ocean areas[28] because of a lack of field data to quantify the occurrence and magnitude of calcium precipitation/dissolution in estuarine environments. The threshold estimated from 20 years of bay-wide water quality data in this study could be incorporated into the process-based physical-biogeochemical models, reducing the biases and uncertainties in carbonate chemistry simulations (e.g., CO_2 sink/source, climate change on estuarine pH).

Coupling and decoupling of hypoxia and acidification in Chesapeake Bay

The coupling of hypoxia and acidification has been observed in diverse aquatic systems, particularly for eutrophic environments,[8,9,57-60] due to the linkage via aerobic respiration. The rates of net biogeochemical DO and DIC production we calculated allow for the investigation of coupled hypoxia and acidification as a function of metabolic processes. A 33-year (1986–2018) record of field observations in Chesapeake Bay demonstrated both hypoxia (DO < 62.5 μM) and acidification (pH < 7.5 NBS) routinely develop in mid-bay bottom waters, and the seasonal patterns for bottom pH and DO clearly reveal the coupling and decoupling of hypoxia and acidification in this vulnerable region (Fig. 5). DO observations display an overall long duration of hypoxia across the whole summer. In contrast, long-term historical pH data display a minimum in June and a quick recovery from the lowest point with notable alleviations on acidification in late summer (July and August). Our box model illustrated a dominant contribution of aerobic respiration to DO and DIC (71%) in the early summer (Fig. 3d), leading to the synchronous declines of DO and pH in May and June, in other words, the

coupling of hypoxia and acidification. The relatively higher non-aerobic-respiration contributions of DIC in late summer (Fig. 3d) suggest the potential for both pH buffering and non-buffering processes in the water column and sediments to alter bottom water pH, including carbonate mineral dissolution under low saturation environments with a ΔTA: ΔDIC ratio of 2.0.

$$CaCO_3 + CO_2 + H_2O \rightarrow Ca^{2+} + 2HCO_3^- \quad (12)$$

and sulfate reduction with a ΔTA: ΔDIC ratio of 1.14.

$$(CH_2O)_{106}(NH_3)_{16}H_3PO_4 + 53SO_4^{2-} \rightarrow 53H_2S + 106HCO_3^- + H_3PO_4 + 16NH_3 \quad (13)$$

Carbonate mineral dissolution has the potential for buffering of low pH in bottom mid Bay under hypoxic/anoxic environments established during summer. These processes could potentially alter the coupling of hypoxia and acidification in late summer. Although these biogeochemical processes have not or rarely been directly measured and quantified in Chesapeake Bay, recent field studies and process-based model simulations all implied key roles of dissolution in buffering water from continuous pH decline in August.[25,28,54] In particular, Su et al.[30] analyzed a year's worth of DIC, TA, and Ca^{2+} distributions with a two-endmember mixing approach in Chesapeake Bay and concluded that $CaCO_3$ dissolution accounted for the major changes of DIC (<40% in our study, Fig. 3d). Because this dissolution signal did not emerge until August, well after Ω_{ar} dropped below 1.0 (new threshold of 0.64 generated in this study, Fig. 4), Su et al. concluded that dissolution was supply-controlled and possibly linked to calcification originating in macrophyte communities.

Impacts of nutrient inputs on hypoxia and acidification

Questions remain as to how the decoupling between hypoxia and acidification identified in this and previous studies varies with interannual changes in external forcing, and how external forcing relates to possible $CaCO_3$ production sources. Average Susquehanna River nutrient loading during January–May was tightly correlated with hypoxic volumes during the following June, July, and August (Fig. 6), suggesting that nutrient loading and eutrophication are the main drivers for the interannual variability of hypoxia in Chesapeake Bay, as found in previous studies.[61-63] Recent model sensitivity scenarios implied positive correlations between

the external nutrient loading and acidified volumes in Chesapeake Bay.[28] In this study, the acidified volumes for June between 1999 and 2018 also increase with nutrient loading. However, no significant correlations were observed between acidified volumes and nutrient loading in July and acidified volumes in August showed a negative relationship to nutrient loading. Thus, the hypoxic and acidified volumes based on field observations indicate the dominance of aerobic respiration during early summer (i.e., June), leading to the coupling of hypoxia and acidification, followed by the decoupling of hypoxia and acidification in July and August.

The decoupling of eutrophication-induced deoxygenation and acidification in late summer in Chesapeake Bay is consistent with recent hypotheses.[30] A possible mechanism is that nutrient inputs stimulate the generation and transport of $CaCO_3$ that later supports carbonate dissolution and alkalinity generation in hypoxic bottom waters. Recent reports have suggested that $CaCO_3$ dissolution is a dominant contributor of alkalinity in Chesapeake Bay in late summer, which can elevate pH,[30] but there is no evidence that this dissolution occurs at higher rates in years of elevated nutrient loading. Su et al.[25] suggested that submerged macrophyte beds stimulate $CaCO_3$ production, but these beds are usually less productive (and thus likely generate less $CaCO_3$) in years of high riverine inflows.[64] Planktonic $CaCO_3$ production is well known in some phytoplankton communities, and nutrient inputs could stimulate the growth of these organisms, but no direct measurements of such production have been reported for this estuary. Furthermore, many species of foraminifera have been reported in Chesapeake Bay and its tributaries,[65] but it is unclear if riverine inputs or associated elevated advection rates would stimulate foraminifera-derived calcification following transport to (or accumulation in) mainstem deep waters. A mechanism that could slow the pH decline expected from organic matter decomposition in late summer is that elevated nutrient loads enhance the extent and severity of anoxia that develops in mid-summer and the associated sulfide accumulation[19, 25, 37]. The accumulation of sulfide in bottom water could temporarily delay the pH reduction expected from sulfide oxidation or spatially decouple sulfide oxidation (which occurs above the pycnocline) from low-pH bottom waters. Furthermore, a portion of the sulfide generated from sulfate reduction is buried or temporarily stored in sediments[66], delaying or limiting its oxidation. Clearly there is a need for additional

measurements and model simulations to understand the mechanisms behind the decoupled hypoxic and acidified volumes, given the uncertainty in the source processes, the relevant environmental controls, and its importance for our understanding of estuarine acidification.

Management implications

Hypoxia and its relationship to nutrient loading has been intensively studied in Chesapeake Bay for several decades. Multiple efforts to improve the Bay's water quality eventually resulted in the 2010 Chesapeake Bay Total Maximum Daily Load, which reduced nutrient inputs from point sources and non-point sources into the Bay.[31,61] Strong correlations between winter–spring nutrient loading and hypoxic volumes across the summer suggest that continuous watershed restrictions on nutrient loading would be effective to alleviate hypoxia in the mainstem. Prior work has associated reduced nutrient loads with lower respiration, having the effect of alleviating bottom water acidification.[8,28] Thus, nutrient remediation targeting hypoxia may have the unintended benefit of reducing acidification. However, the seasonal decoupling between hypoxia and acidification in late summer noted in this study reveals that the relationship between external loading and bottom-water acidification may be more complex. Given that eutrophication mitigation is not the only management option available to address acidification, other forms of buffering estuarine water should be considered. Besides management efforts to reduce CO_2 emissions, regional management strategies aimed at restoring bay-wide submerged aquatic vegetation could also have the benefit of offsetting acidification by drawing down DIC and promoting carbon sequestration. Meanwhile, bottom waters are widely corrosive in early summer, particularly for wet years. The wind-driven lateral upwelling could expose the local native eastern oysters in shallow shoals to episodic acidic conditions. The late-summer buffering from our study implies that management activities to return old crashed shells to the hatchery sites in late spring and early summer could increase the aragonite saturation condition state and oyster survivorship through calcium dissolution.

Carbonate chemistry varies spatially and temporally in Chesapeake Bay, but the full extent of that variation has not been thoroughly explored because the carbonate system variables have not been widely measured. Limited field observations in recent years suggest

strong influences of diurnal and tidal cycling, as well as strong seasonal variations.[26,40] Seasonal and interannual dynamics need to be placed in a long-term context through observation with the goal of understanding how such patterns may be trending through time. Given the widespread research and monitoring taking place across Chesapeake Bay and other estuaries, there are extensive opportunities for adding observations and measurements (e.g., pCO_2, DIC, and TA) aimed at characterizing the dynamics and mechanistic drivers of carbonate chemistry and estuarine acidification. Additional observations and research efforts could leverage Chesapeake Bay's existing infrastructure and monitoring programs (e.g., existing water quality stations, water quality and oceanographic cruises), thereby rapidly increasing carbonate chemistry measurements and our knowledge about estuarine acidification at local and regional scales. Monitoring in estuarine environments would ideally be conducted with higher frequencies to cover short-term variability, with higher horizontal and vertical resolutions to understand how physical mixing, circulation and biological processes would impact acidification along the salinity gradient, and with multiple parameters measured to characterize and understand acidification more thoroughly. Data collected from these monitoring programs could be used to investigate underlying mechanisms and establish empirical relationships, which may also inform the study of acidification in other riverine and estuarine systems. In all, acidification monitoring across the United States and other regions in the world is very limited but increasing quickly, emphasizing the leveraging of existing monitoring and structures, particularly those aimed for hypoxia, eutrophication and harmful algal blooms.

Supporting Information

USGS gage stations used for freshwater inputs and CBP water quality stations used for computing tributary salinity; diagram of box model for Chesapeake Bay; Two-dimensional depth-length grid along the mainstem Bay used for interpolation; Long-term monthly average particulate organic carbon concentration measured in bottom waters at mid-bay region.

Acknowledgement

We would like to thank Wei-Jun Cai for his insightful comments and general guidance on this study. This study was funded by the United States National Oceanographic and Atmospheric Administration Ocean Acidification Program (NOAA-OAP; award # NA15NOS4780184) and National Science Foundation (OCE-1536996). We also thank the US EPA Chesapeake Bay Program, Maryland Department of Natural Resources, and United States Geological Survey for water monitoring data utilized in this study. This is UMCES contribution number XXXX.

Reference

(1) Doney, S.C.; Fabry, V.J.; Feely, R.A.; Kleypas, J.A. Ocean acidification: The other CO_2 problem. *Annual Review of Marine Science* **2009**, *1*, pp.169-192.

(2) Feely, R.A.; Sabine, C.L.; Lee, K.; Berelson, W.; Kleypas, J.; Fabry, V.J.; Millero, F.J. Impact of anthropogenic CO_2 on the $CaCO_3$ system in the oceans. *Science* **2004**, *305*(5682), pp.362-366.

(3) Feely, R.A.; Doney, S.C.; Cooley, S.R. Ocean acidification: Present conditions and future changes in a high-CO_2 world. *Oceanography* **2009**, *22*(4), pp.36-47.

(4) Hagens, M.; Slomp, C.P.; Meysman, F.J.R.; Seitaj, D.; Harlay, J.; Borges, A.V.; Middelburg, J.J. Biogeochemical processes and buffering capacity concurrently affect acidification in a seasonally hypoxic coastal marine basin. *Biogeosciences* **2015**, *12*(5), pp.1561-1583.

(5) Najjar, R.G.; Herrmann, M.; Del Valle S.M.C.; Friedman, J.R.; Friedrichs, M.A.; Harris, L.A.; Shadwick, E.H.; Stets, E.G.; Woodland, R.J. Alkalinity in tidal tributaries of the Chesapeake Bay. *Journal of Geophysical Research: Oceans* **2020**, *125*, e2019JC015597.

(6) Kaushal, S.S.; Likens, G.E.; Utz, R.M.; Pace, M.L.; Grese, M. and Yepsen, M. Increased river alkalinization in the Eastern US. *Environmental Science & Technology*, **2013**, *47*(18), pp.10302-10311.

(7) Rheuban, J.E.; Gassett, P.R.; McCorkle, D.C.; Hunt, C.W.; Liebman, M.; Bastidas, C.; O'Brien-Clayton, K.; Pimenta, A.R.; Silva, E.; Vlahos, P. and Woosley, R.J. Synoptic assessment of coastal total alkalinity through community science. *Environmental Research Letters* **2021**, *16*(2), p.024009.

(8) Cai, W.J.; Hu, X.; Huang, W.J.; Murrell, M.C.; Lehrter, J.C.; Lohrenz, S.E.; Chou, W.C.; Zhai, W.; Hollibaugh, J.T.; Wang, Y.; Zhao, P. Acidification of subsurface coastal waters enhanced by eutrophication. *Nature Geoscience* **2011**, *4*(11), pp.766-770.

(9) Wallace, R.B.; Baumann, H.; Grear, J.S.; Aller, R.C.; Gobler, C.J. Coastal ocean acidification: The other eutrophication problem. *Estuarine, Coastal and Shelf Science* **2014**, *148*, pp.1-13.

(10) Waldbusser, G.G.; Voigt, E.P.; Bergschneider, H.; Green, M.A.; Newell, R.I. Biocalcification in the eastern oyster (Crassostrea virginica) in relation to long-term trends in Chesapeake Bay pH. *Estuaries and Coasts* **2011**, *34*(2), pp.221-231.

(11) Carstensen, J.; Andersen, J.H.; Gustafsson, B.G.; Conley, D.J. Deoxygenation of the Baltic Sea during the last century. *Proceedings of the National Academy of Sciences* **2014**, *111*(15), pp.5628-5633.

(12) Neumann, T.; Radtke, H.; Seifert, T. On the importance of Major Baltic Inflows for oxygenation of the central Baltic Sea. *Journal of Geophysical Research: Oceans* **2017**, *122*(2), pp.1090-1101.

(13) Laurent, A.; Fennel, K.; Cai, W.J.; Huang, W.J.; Barbero, L.; Wanninkhof, R. Eutrophication-induced acidification of coastal waters in the northern Gulf of Mexico: Insights into origin and processes from a coupled physical-biogeochemical model. *Geophysical Research Letters* **2017**, *44*(2), pp.946-956.

(14) Scavia, D.; Donnelly, K.A. Reassessing hypoxia forecasts for the Gulf of Mexico. *Environmental Science & Technology* **2007**, *41*(23), pp.8111-8117.

(15) Dai, M.; Guo, X.; Zhai, W.; Yuan, L.; Wang, B.; Wang, L.; Cai, P.; Tang, T.; Cai, W.J. Oxygen depletion in the upper reach of the Pearl River estuary during a winter drought. *Marine Chemistry* **2006**, *102*(1-2), pp.159-169.
(16) Yu, L.; Gan, J. Mitigation of eutrophication and hypoxia through oyster aquaculture: An ecosystem model evaluation off the Pearl River estuary. *Environmental Science & Technology* **2021**, *55*(8), pp.5506-5514.
(17) Testa, J.M.; Clark, J.B.; Dennison, W.C.; Donovan, E.C.; Fisher, A.W.; Ni, W.; Parker, M.; Scavia, D.; Spitzer, S.E.; Waldrop, A.M.; Vargas, V.M. Ecological forecasting and the science of hypoxia in Chesapeake Bay. *BioScience* **2017**, *67*(7), pp.614-626.
(18) Duarte, C.M.; Dennison, W.C.; Orth, R.J.; Carruthers, T.J. The charisma of coastal ecosystems: addressing the imbalance. *Estuaries and Coasts* **2008**, *31*(2), pp.233-238.
(19) Murphy, R.R.; Kemp, W.M.; Ball, W.P. Long-term trends in Chesapeake Bay seasonal hypoxia, stratification, and nutrient loading. *Estuaries and Coasts* **2011**, *34*(6), pp.1293-1309.
(20) Scavia, D., Bertani, I., Obenour, D.R., Turner, R.E., Forrest, D.R. and Katin, A. Ensemble modeling informs hypoxia management in the northern Gulf of Mexico. *Proceedings of the National Academy of Sciences* **2017**, *114*(33), pp.8823-8828.
(21) Fennel, K.; Testa, J.M. Biogeochemical controls on coastal hypoxia. *Annual Review of Marine Science* **2019**, *11*, pp.105-130.
(22) Gobler, C.J.; Baumann, H. Hypoxia and acidification in ocean ecosystems: coupled dynamics and effects on marine life. *Biology Letters* **2016**, *12*(5), p.20150976.
(23) Gobler, C.J.; DePasquale, E.L.; Griffith, A.W.; Baumann, H. Hypoxia and acidification have additive and synergistic negative effects on the growth, survival, and metamorphosis of early life stage bivalves. *PLOS ONE* **2014**, *9*(1), e83648.
(24) Carstensen, J.; Duarte, C.M. Drivers of pH variability in coastal ecosystems. *Environmental Science & Technology* **2019**, *53*(8), pp.4020-4029.
(25) Su, J.; Cai, W.J.; Brodeur, J.; Chen, B.; Hussain, N.; Yao, Y.; Ni, C.; Testa, J.M.; Li, M.; Xie, X.; Ni, W. Chesapeake Bay acidification buffered by spatially decoupled carbonate mineral cycling. *Nature Geoscience* **2020**, *13*(6), pp.441-447.
(26) Brodeur, J.R.; Chen, B.; Su, J.; Xu, Y.Y.; Hussain, N.; Scaboo, K.M.; Zhang, Y.; Testa, J.M.; Cai, W.J. Chesapeake Bay inorganic carbon: Spatial distribution and seasonal variability. *Frontiers in Marine Science* **2019**, *6*, p.99.
(27) Friedman, J.R.; Shadwick, E.H.; Friedrichs, M.A.; Najjar, R.G.; De Meo, O.A.; Da, F.; Smith, J.L. Seasonal variability of the CO2 system in a large coastal plain estuary. *Journal of Geophysical Research: Oceans* **2020**, *125*(1), e2019JC015609.
(28) Shen, C.; Testa, J.M.; Li, M.; Cai, W.J.; Waldbusser, G.G.; Ni, W.; Kemp, W.M.; Cornwell, J.; Chen, B.; Brodeur, J.; Su, J. Controls on carbonate system dynamics in a coastal plain estuary: A modeling study. *Journal of Geophysical Research: Biogeosciences* **2019**, *124*(1), pp.61-78.
(29) St-Laurent, P.; Friedrichs, M.A.; Najjar, R.G.; Shadwick, E.H.; Tian, H.; Yao, Y. Relative impacts of global changes and regional watershed changes on the inorganic carbon balance of the Chesapeake Bay. *Biogeosciences* **2020**, *17*(14), pp.3779-3796.
(30) Su, J.; Cai, W.J.; Testa, J.M.; Brodeur, J.R.; Chen, B.; Scaboo, K.M.; Li, M.; Shen, C.; Dolan, M.; Xu, Y.Y.; Zhang, Y. Supply-controlled calcium carbonate dissolution decouples the seasonal dissolved oxygen and pH minima in Chesapeake Bay. *Limnology and Oceanography* **2021**, *66*(10), pp.3796-3810.
(31) Testa, J.M.; Kemp, W.M.; Boynton, W.R. Season-specific trends and linkages of nitrogen and oxygen cycles in Chesapeake Bay. *Limnology and Oceanography* **2018**, *63*(5), pp.2045-2064.
(32) Hagy III, J.D. Eutrophication, hypoxia and trophic transfer efficiency in Chesapeake Bay. Doctoral dissertation, University of Maryland, College Park, **2002**.
(33) Li, M.; Zhong, L.; Boicourt, W.C. Simulations of Chesapeake Bay estuary: Sensitivity to turbulence mixing parameterizations and comparison with observations. *Journal of Geophysical Research: Oceans* **2005**, *110*, C12004.
(34) Cerco, C.F.; Noel, M.R. Can oyster restoration reverse cultural eutrophication in Chesapeake Bay? *Estuaries and Coasts* **2007**, *30*(2), pp.331-343.
(35) Murphy, R.R.; Keisman, J.; Harcum, J.; Karrh, R.R.; Lane, M.; Perry, E.S.; Zhang, Q. Nutrient improvements in Chesapeake Bay: Direct effect of load reductions and implications for coastal management. *Environmental Science & Technology* **2021,** *56*(1), pp.260-270.
(36) Lefcheck, J.S.; Orth, R.J.; Dennison, W.C.; Wilcox, D.J.; Murphy, R.R.; Keisman, J.; Gurbisz, C.; Hannam, M.; Landry, J.B.; Moore, K.A.; Patrick, C.J. Long-term nutrient reductions lead to the

unprecedented recovery of a temperate coastal region. *Proceedings of the National Academy of Sciences* **2018**, *115*(14), pp.3658-3662.
(37) Hagy, J.D.; Boynton, W.R.; Keefe, C.W.; Wood, K.V. Hypoxia in Chesapeake Bay, 1950–2001: long-term change in relation to nutrient loading and river flow. *Estuaries* **2004**, *27*(4), pp.634-658.
(38) Testa, J.M.; Li, Y.; Lee, Y.J.; Li, M.; Brady, D.C.; Di Toro, D.M.; Kemp, W.M.; Fitzpatrick, J.J. Quantifying the effects of nutrient loading on dissolved O2 cycling and hypoxia in Chesapeake Bay using a coupled hydrodynamic–biogeochemical model. *Journal of Marine Systems* **2014**, *139*, pp.139-158.
(39) Cowan, J.L. and Boynton, W.R. Sediment-water oxygen and nutrient exchanges along the longitudinal axis of Chesapeake Bay: seasonal patterns, controlling factors and ecological significance. *Estuaries* **1996**, *19*(3), pp.562-580.
(40) Shadwick, E.H.; Friedrichs, M.A.; Najjar, R.G.; De Meo, O.A.; Friedman, J.R.; Da, F.; Reay, W.G. High-frequency CO2 system variability over the winter-to-spring transition in a coastal plain estuary. *Journal of Geophysical Research: Oceans* **2019**, *124*(11), pp.7626-7642.
(41) Wong, G.T. Alkalinity and pH in the southern Chesapeake Bay and the James River estuary 1. *Limnology and Oceanography* **1979**, *24*(5), pp.970-977.
(42) Herrmann, M.; Najjar, R.G.; Da, F.; Friedman, J.R.; Friedrichs, M.A.; Goldberger, S.; Menendez, A.; Shadwick, E.H.; Stets, E.G.; St-Laurent, P. Challenges in quantifying air-water carbon dioxide flux using estuarine water quality data: Case study for Chesapeake Bay. *Journal of Geophysical Research: Oceans* **2020**, *125*(7), e2019JC015610.
(43) Van Heuven, S.M.A.C.; Pierrot, D.; Rae, J.W.B.; Lewis, E.; Wallace, D.W.R. MATLAB Program developed for CO2 system calculations, ORNL/CDIAC-105b. *Carbon Dioxide Information Analysis Center, Oak Ridge National Laboratory, US Department of Energy, Oak Ridge, Tennessee* **2011**, *530*.
(44) Cai, W.J.; Wang, Y. The chemistry, fluxes, and sources of carbon dioxide in the estuarine waters of the Satilla and Altamaha Rivers, Georgia. *Limnology and Oceanography* **1998**, *43*(4), pp.657-668.
(45) Dickson, A.G. Thermodynamics of the dissociation of boric acid in synthetic seawater from 273.15 to 318.15 K. *Deep Sea Research Part A. Oceanographic Research Papers* **1990**, *37*(5), pp.755-766.
(46) Uppström, L.R. The boron/chlorinity ratio of deep-sea water from the Pacific Ocean. *Deep Sea Res* **1974**. *21*, 161–162.
(47) Diggle, P.J.; Tawn, J.A. and Moyeed, R.A. Model-based geostatistics. *Journal of the Royal Statistical Society: Series C (Applied Statistics)* **1998**, *47*(3), pp.299-350.
(48) Garcia, H.E.; Gordon, L.I. Oxygen solubility in seawater: Better fitting equations. *Limnology and Oceanography* **1992**, *37*(6), pp.1307-1312.
(49) Weiss, R. Carbon dioxide in water and seawater: The solubility of a non-ideal gas. *Marine Chemistry* **1974**, *2*(3), pp.203-215.
(50) Wanninkhof, R. Relationship between wind speed and gas exchange over the ocean revisited. *Limnology and Oceanography: Methods* **2014**, *12*(6), pp.351-362.
(51) Redfield, A.C. The influence of organisms on the composition of seawater. *The sea* **1963**, 2, pp.26-77.
(52) Malone, T.C. Effects of water column processes on dissolved oxygen: Nutrients, plankton and zooplankton. In *Oxygen dynamics in Chesapeake Bay: A synthesis of research*. College Park: University of Maryland Sea Grant College Publications, **1992**, 61-112.
(53) Kemp, W.M.; Smith, E.M.; Marvin-DiPasquale, M.; Boynton, W.R. Organic carbon balance and net ecosystem metabolism in Chesapeake Bay. *Marine Ecology Progress Series* **1997**, *150*, pp.229-248.
(54) Cai, W.J.; Huang, W.J.; Luther, G.W.; Pierrot, D.; Li, M.; Testa, J.; Xue, M.; Joesoef, A.; Mann, R.; Brodeur, J.; Xu, Y.Y. Redox reactions and weak buffering capacity lead to acidification in the Chesapeake Bay. *Nature Communications* **2017**, *8*(1), pp.1-12.
(55) Mucci, A. The solubility of calcite and aragonite in seawater at various salinities, temperatures, and one atmosphere total pressure. *American Journal of Science* **1983**, *283*(7), pp.780-799.
(56) Da, F., Friedrichs, M.A., St-Laurent, P., Shadwick, E.H., Najjar, R.G. and Hinson, K.E. Mechanisms driving decadal changes in the carbonate system of a coastal plain estuary. *Journal of Geophysical Research: Oceans* **2021**, *126*(6), p.e2021JC017239.
(57) Baumann, H.; Wallace, R.B.; Tagliaferri, T.; Gobler, C.J. Large natural pH, CO2 and O2 fluctuations in a temperate tidal salt marsh on diel, seasonal, and interannual time scales. *Estuaries and Coasts* **2015**, 38(1), pp.220-231.

(58) Baumann, H.; Smith, E.M. Quantifying metabolically driven pH and oxygen fluctuations in US nearshore habitats at diel to interannual time scales. *Estuaries and Coasts* **2018**, *41*(4), pp.1102-1117.
(59) Mucci, A.; Starr, M.; Gilbert, D.; Sundby, B. Acidification of lower St. Lawrence Estuary bottom waters. *Atmosphere-Ocean* **2011**, *49*(3), pp.206-218.
(60) Zhao, Y.; Liu, J.; Uthaipan, K.; Song, X.; Xu, Y.; He, B.; Liu, H.; Gan, J.; Dai, M. Dynamics of inorganic carbon and pH in a large subtropical continental shelf system: Interaction between eutrophication, hypoxia, and ocean acidification. *Limnology and Oceanography* **2020**, *65*(6), pp.1359-1379.
(61) Scavia, D.; Bertani, I.; Testa, J.M.; Bever, A.J.; Blomquist, J.D.; Friedrichs, M.A.; Linker, L.C.; Michael, B.D.; Murphy, R.R.; Shenk, G.W. Advancing estuarine ecological forecasts: Seasonal hypoxia in Chesapeake Bay. *Ecological Applications* **2021**, p.e2384.
(62) Harding Jr, L.W.; Adolf, J.E.; Mallonee, M.E.; Miller, W.D.; Gallegos, C.L.; Perry, E.S.; Johnson, J.M.; Sellner, K.G.; Paerl, H.W. Climate effects on phytoplankton floral composition in Chesapeake Bay. *Estuarine, Coastal and Shelf Science* **2015**, *162*, pp.53-68.
(63) Li, M.; Lee, Y.J.; Testa, J.M.; Li, Y.; Ni, W.; Kemp, W.M.; Di Toro, D.M. What drives interannual variability of hypoxia in Chesapeake Bay: Climate forcing versus nutrient loading? *Geophysical Research Letters* **2016**, *43*(5), pp.2127-2134.
(64) Orth, R.J.; Dennison, W.C.; Lefcheck, J.S.; Gurbisz, C.; Hannam, M.; Keisman, J.; Landry, J.B.; Moore, K.A.; Murphy, R.R.; Patrick, C.J.; Testa, J. Submersed aquatic vegetation in Chesapeake Bay: sentinel species in a changing world. *Bioscience* **2017**, *67*(8), pp.698-712.
(65) Ellison, R.L.; Nichols, M.M. Ecology of foraminifera from the Rappahannock Estuary, Virginia. *Cushman Foundation for Foraminiferal Research Contributions* **1970**, *21*:1–17.
(66) Cornwell, J.C.; Sampou, P.A. Environmental controls on iron sulfide mineral formation in a coastal plain estuary. In: *Vairavamurthy MA, Schoonen MAA (eds) Geochemical transformations of sedimentary sulfur*. American Chemical Society, Washington, DC, **1995**, p 224–242

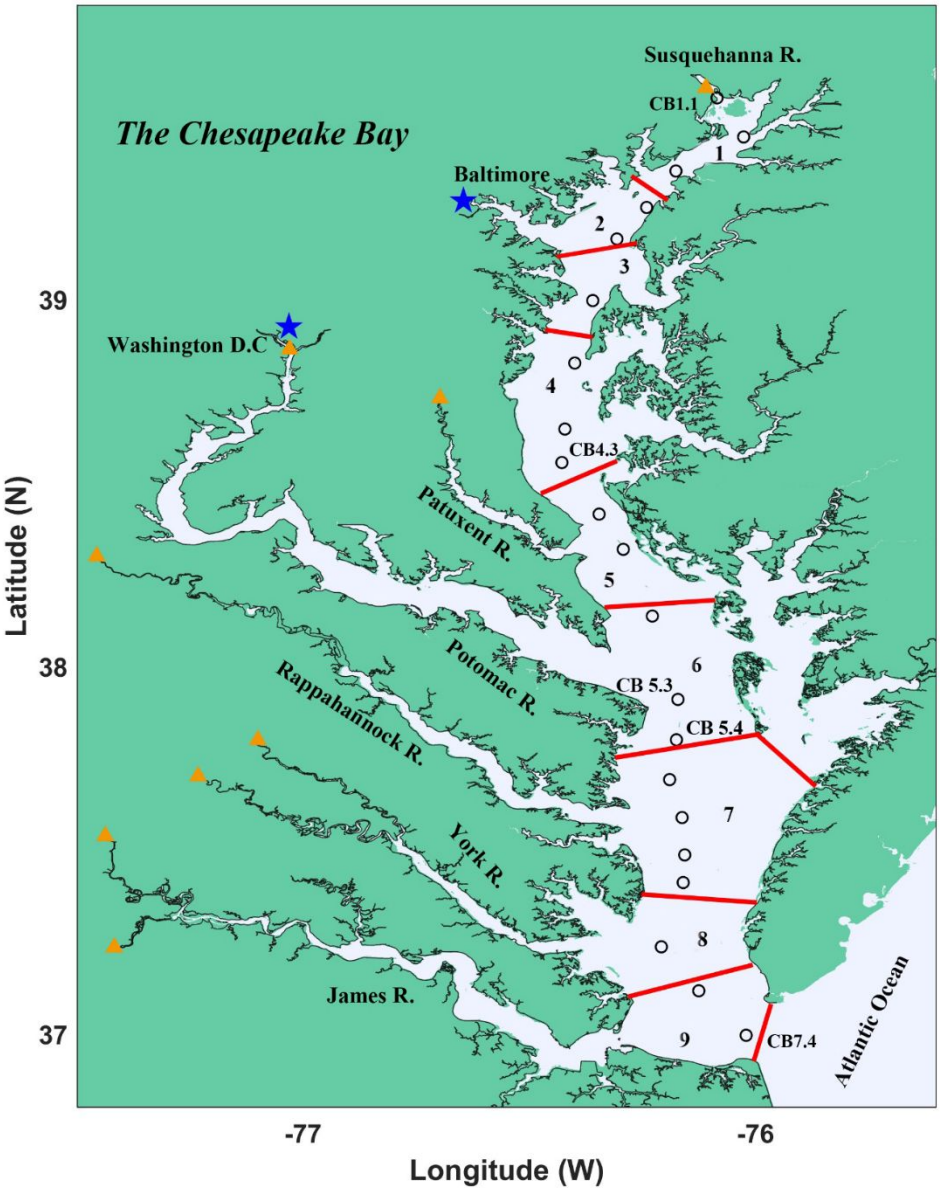

Fig. 1. Map of Chesapeake Bay, including boundaries (red lines) of box-model regions (numbered), tributary rivers, the Chesapeake Bay Program sampling stations (white circles), and the USGS gage stations (yellow triangles).

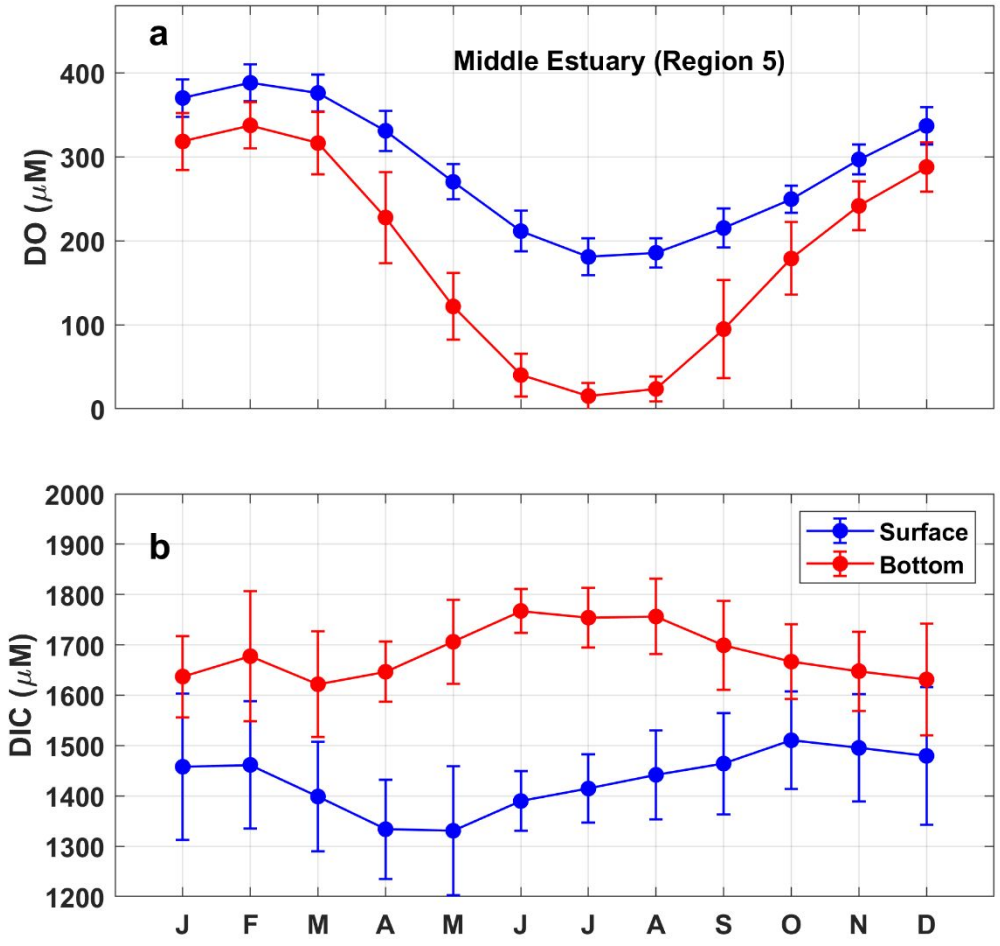

Fig. 2. Monthly climatological averages of (a) dissolved oxygen and (b) dissolved inorganic carbon in surface and bottom of the middle estuary (Region 5). The bars represent one standard deviation of the 20-year mean (1999–2018).

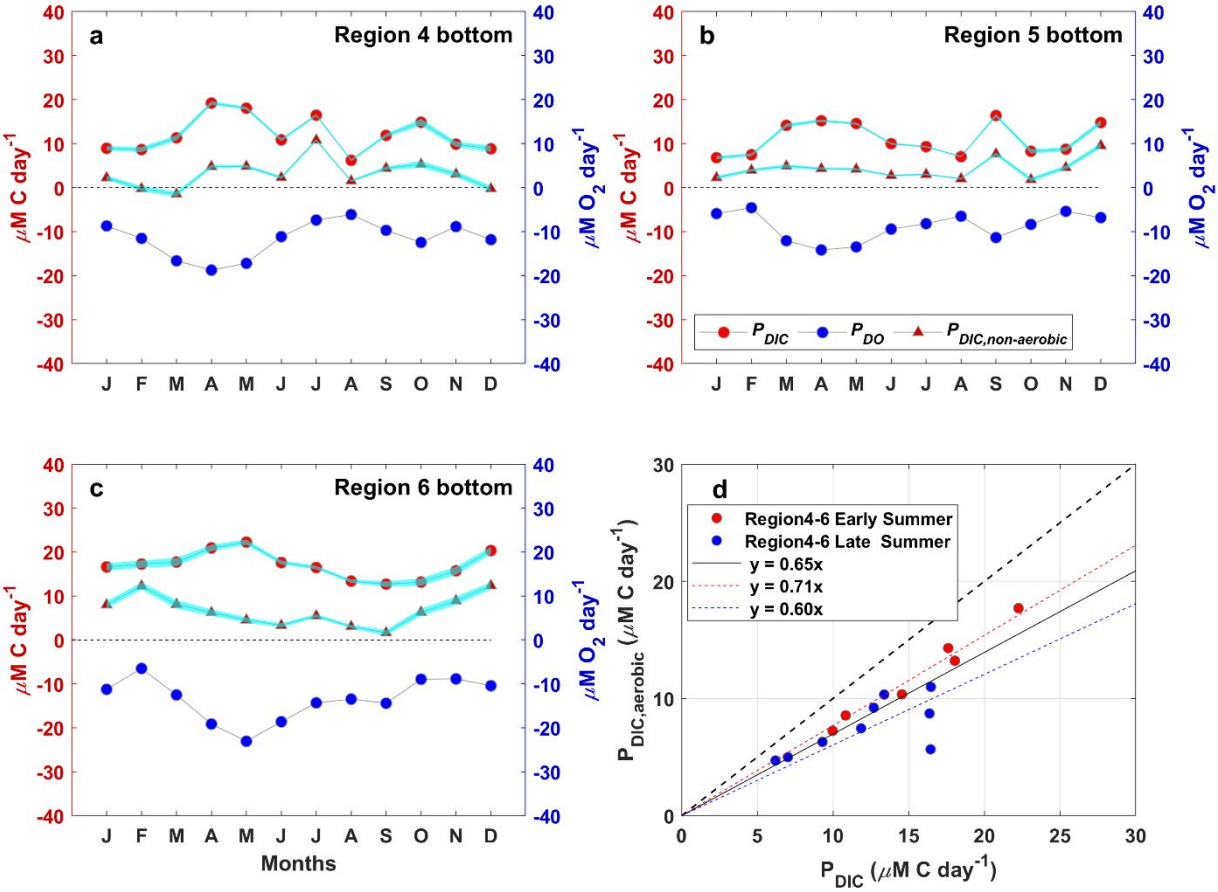

Fig. 3. Monthly climatological averages (1999–2018) of net biogeochemical production rates for DO (P_{DO}) and DIC (P_{DIC}) inferred from the box-model calculation in bottom of (a) Region 4, (b) Region 5, and (c) Region 6. Also shown is the estimated (see text) non-aerobic-respiration-induced DIC production ($P_{DIC,\ non\text{-}aerobic}$). (d) Comparisons between 1999–2018 mean net DIC production (P_{DIC}) and aerobic-respiration-induced DIC production ($P_{DIC,aerobic}$) in both early summer (May–June) and late summer (July–September). Shaded area in panels a–c represents the 95% confidence range on P_{DIC} and $P_{DIC,\ non\text{-}aerobic}$ from the 200-simulation Monte Carlo ensemble.

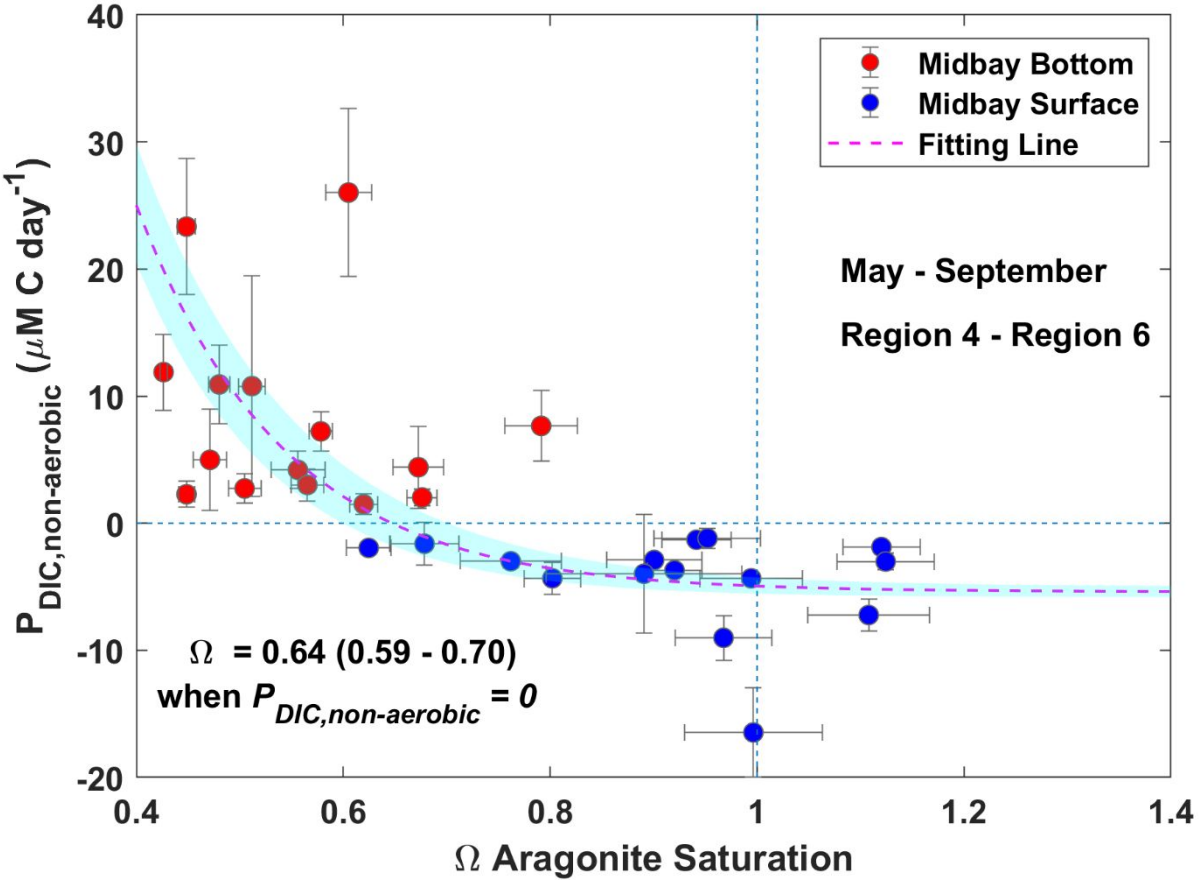

Fig. 4. DIC production due to non-aerobic respiration ($P_{DIC,\ non\text{-}aerobic}$) vs. aragonite saturation state averaged over Regions 4 to 6 in both surface and bottom boxes over the May to September period. The bars represent one standard deviation of the 1999–2018 mean. The pink line represents the best-fit exponential function. The shaded area shows the 95% confidence range of the 200-simulation Monte Carlo ensemble.

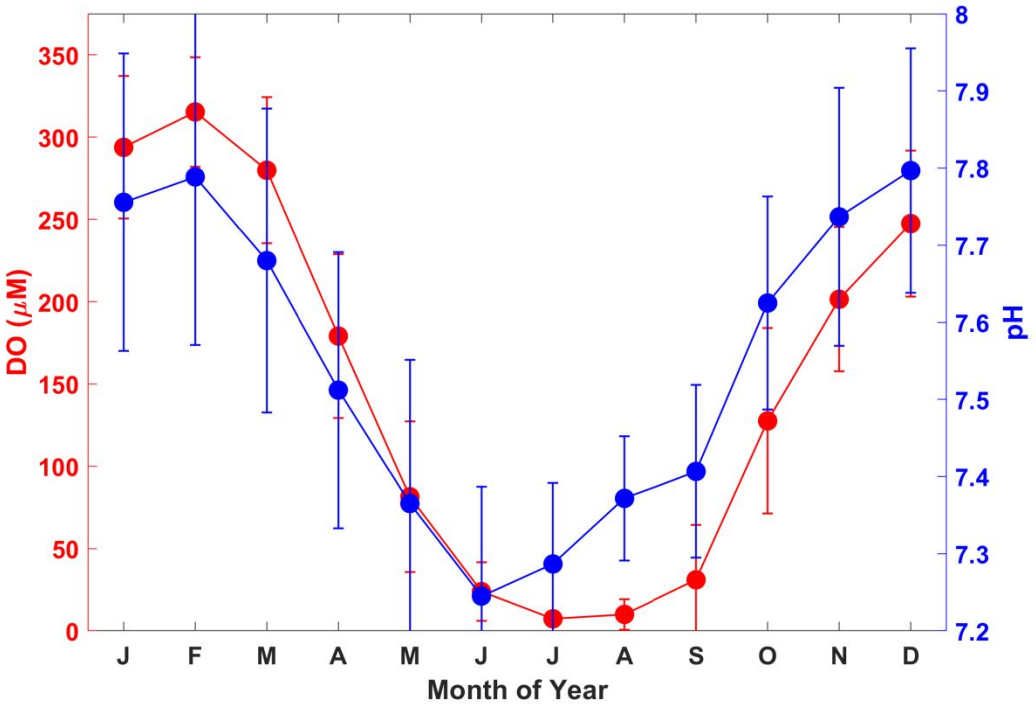

Fig. 5. Long-term (1986-2018) monthly average DO and pH measured in bottom waters at mid-bay region (Region 5). The bars represent one standard deviation.

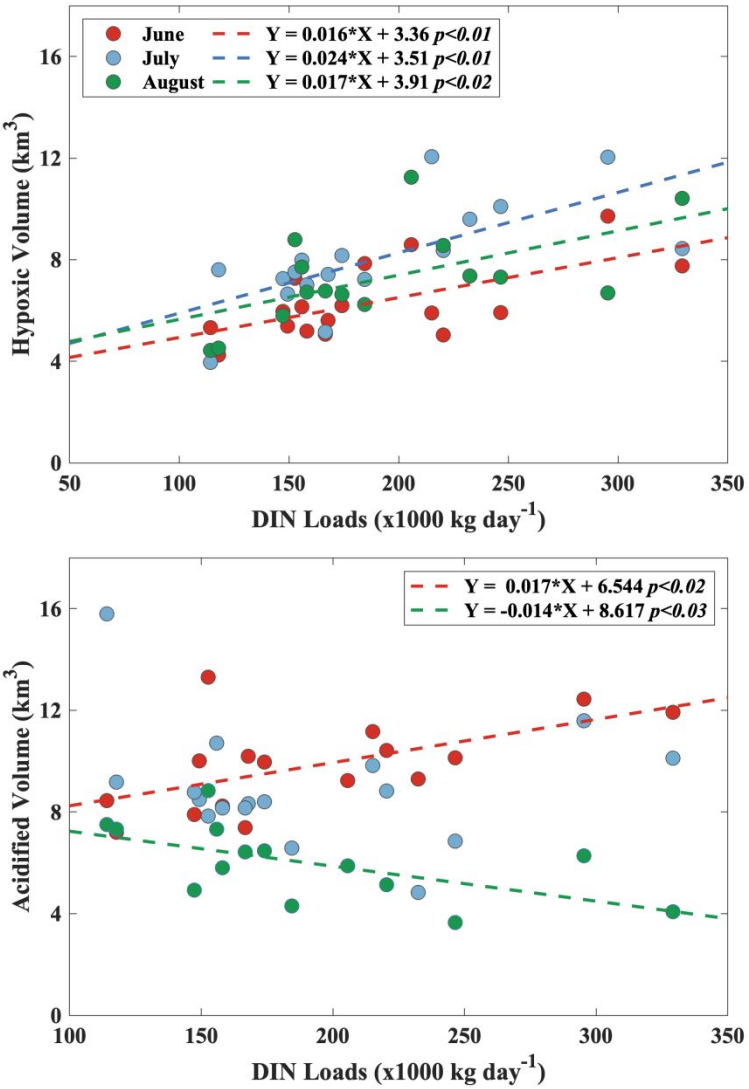

Fig. 6. Correlations between winter–spring (January to May) total inorganic nitrogen loads and monthly estimates of (top) hypoxic volume and (bottom) acidified volume for June, July, and August. The dashed lines represent linear regression best fits for those relationships with a *p*-value less than 0.05.